Intercomparison of the June 2013 Southwest Alberta rainstorm with past heavy precipitation events

Part 2 of Weather Analysis Project for

Canmore's Mountain Creek Hazard Mitigation

March 14, 2014

Town of Canmore

[redacted]

Principal Investigator:
Prof. Roland Stull, PMet, CCM, CFII
Earth, Ocean & Atmos. Sci. Dept.
University of British Columbia
2020-2207 Main Mall
Vancouver BC, V6T 1Z4
phone: 604-822-5901, fax: 604-822-6088
email: rstull@eos.ubc.ca

Report created by:
Dr. Rosie Howard
Earth, Ocean & Atmos. Sci. Dept.
University of British Columbia
2020-2207 Main Mall
Vancouver BC, V6T 1Z4
phone: 604-822-5901, fax: 604-822-6088
email: rhoward@eos.ubc.ca

Executive Summary

Heavy precipitation caused severe flooding in Canmore and surrounding area in June 2013, affecting tens of thousands of residents in southwest Alberta. Precipitation data was used to identify similar events (18 total for the period 1952–2013), to investigate whether

the synoptic conditions causing them have changed, and whether there is any relationship with large-scale climate signals.

Reanalysis data from the National Centers for Environmental Prediction/National Center for Atmospheric Research was used to score each event according to the main mechanisms that are known to lead to heavy precipitation in southwest Alberta. Since no correlation was found between precipitation amounts and the resulting scores, we conclude that several different combinations of synoptic weather features can cause heavy precipitation.

The scoring system served to classify the storms. Most heavy precipitation events are caused by an upper-level quasi-stationary low-pressure system, with the next most important factors being subtropical moisture source(s), easterly upslope flow, thunderstorms, and frontal precipitation. There is a potential shift in the large-scale pattern, with half the storms after 1990 tapping a subtropical moisture source, four of which included moisture from both the Pacific and the Gulf of Mexico. Some disparity between the scoring and precipitation amounts can be attributed to the subjective nature of the scoring system, as well as the fact that thunderstorms (instability) are not well-modelled by the coarse-resolution reanalysis data.

The return period of heavy precipitation events has decreased from about 6 years in the 1980s to about 3 years presently, meaning that the probability of a heavy precipitation event occurring this year is roughly 1/3.

Very little correlation was found between El Niño Southern Oscillation/Pacific Decadal Oscillation and heavy precipitation events. While there is evidence in the literature for relationships between climate signals and precipitation response in southwest Canada, these mainly exist in the winter and for more stratified than convective storms. All heavy precipitation events in this study occurred between April and September, and since thunderstorms contributed substantially to precipitation totals, the lack of correlation is not surprising.

1. Introduction

In June 2013, heavy precipitation occurred in southwest Alberta (AB), Canada, causing extreme flooding on the Bow River, affecting Banff, Canmore, Calgary, and other residential areas. A first report summarizing the synoptic weather conditions leading to this event determined that during the period 18–21 June 2013, three low-pressure systems interacted to bring very humid air to Southwest AB. This moisture originated from both the Pacific and the Gulf of Mexico, and the local prevailing (easterly) wind direction triggered orographic clouds, heavy up-slope precipitation, and embedded thunderstorms.

This report compares the June 2013 storm with past storms in order to determine whether there has been a long-term change in the large-scale configuration of storms producing heavy precipitation on the eastern slopes of the AB Rockies. Namely, we attempt to determine whether past synoptic conditions leading to heavy precipitation events show any trend, temporally and spatially.

2. Data

a. Precipitation data

Historical precipitation data (EnvironmentCanada 2013) from the three Environment Canada (EC) automatic weather stations closest to the town of Canmore (Banff, Bow Valley, and Kananaskis; see fig. 1) are used. Table 1 outlines the locations and data records for each station, located on or near the eastern slopes of the Rockies. We define a threshold for heavy precipitation events where total rainfall $\geq$ 50 mm/(2 days).

We focus on the synoptic scale, the scale of low-pressure systems and their associated fronts. The predictability of convective, isolated thunder showers (i.e. mesoscale) is less than that of frontal or organized precipitation, so we chose events where at least two of the three stations had recorded a heavy precipitation event for the same time period or within one day of each other, in order to exclude thunderstorms. This criteria produced 18 cases (or "heavy precipitation events") spanning the years 1952–2013 (fig. 2 and table 2). In an attempt to account for instrument changes and inaccuracies over this long period, the Adjusted and Homogenized Canadian Climate Dataset was considered, outcomes of which are discussed in appendix A.

There were 4 cases with total rainfall $\geq$ 50 mm/(2 days) at all three stations, and the remaining 14 cases had the heavy rain at two stations with some rain at the third "drier" station. Precipitation totals for each of the 18 cases lie between 50–100 mm per event, except for those occurring in 2005 and 2013 which have greater amounts (fig. 3). In general, of the three stations, Kananaskis had the most precipitation per event. All cases occurred between April and September (none in July), with the most occurring in May (4 cases) and June (10 cases).

b. Reanalysis data

Analysis of the June 2013 storm was produced using surface and mid-troposphere (50 kPa, roughly 5.5 km above mean sea level) weather analysis maps from EC (see report 1). Similar maps allowing comparison were only available from 2007 onwards, so instead we used data from the National Centers for Environmental Prediction/National Center for Atmospheric Research (NCEP/NCAR) reanalysis project (Kalnay et al. 1996).

This is a global data assimilation system complete with land surface, ship, rawinsonde, aircraft, satellite, and other observations, producing analyses of atmospheric fields over the period 1950–present. We chose six fields to compare with the analysis plots for the June 2013 storm (Godfrey 2010; NCEP/NCAR 2014): geopotential heights at 50 kPa, mean sea level pressure, wind speed and direction interpolated to a near-surface reference pressure of 100 kPa, best 4-layer lifted index (a measure of atmospheric stability), precipitable water, and corrected precipitation rate. Definitions and details of each variable are given in appendix B. Multiple plots (using the available 00Z and 12Z times) covering each event were analyzed in order to view the development of features, e.g. storm speed, lowest pressure centre, moisture source, prevailing winds, etc.

3. Data analysis

a. Spatial analysis

Heavy precipitation in the AB Rockies can be brought about by one or a combination of the following factors (G. West, 2014, pers. comm.):

- **Closed low at 50 kPa** advecting Pacific moisture towards the Canadian Rockies. Deeper and slower-moving closed lows tend to bring the largest amounts of precipitation, having more time to both destabilize the atmosphere and transport moisture. A typical storm will move from southwest to southeast British Columbia (BC) in about 12 hours, but these quasi-stationary storms tend to linger around Washington and Oregon. They are typical in May and June.

- Quasi-stationary surface low-pressure system or troughing in lee of Rocky Mountains, leading to **easterly upslope flow** in the AB Rockies. These systems have been observed transporting monsoonal moisture from southern US, even the Gulf of Mexico (e.g. the June 2013 Canmore storm).

- Progressive (faster-moving) low-pressure system with associated **frontal precipitation**.

- **Thunderstorms** either embedded in fronts and/or triggered by upslope flow.

With these features in mind, each of the 18 heavy precipitation events was "scored" according to which factors they included, as follows (scoring points are in parentheses):

a. Upper-level low (1), slow-moving (+1), low centre $\leq$ 5,500 m (+0.5).

b. Upper-level trough (1).

c. Surface closed low (1), quasi-stationary and centred over Canmore (+0.5), low centre $\leq$ 99.8 kPa (+0.5), surface trough with axis near Canmore (+0.5).

d. Surface trough with front (1) (can score with c **or** d, not both).

e. Easterly component to flow at upper level (0.5), and/or at lower level (0.5).

f. Precipitable water: $\geq$ 20 kg m^{-2} during greatest storm precipitation (1), and/or from a subtropical source: Gulf of Mexico (0.5) and/or Pacific (0.5).

g. Atmospheric stability (to represent thunderstorms): lifted index < 0°C (0.5) or lifted index < -3°C (1).

For example, the April 2003 storm scored 2.5 for feature 'a', having a slow-moving upper-level low with centre reaching 5,350 m (fig. 4). The June 1952 storm scored 2.5 for feature 'c', having a surface low pressure system lingering over Canmore, with central pressure 99.5 kPa, and a surface trough with the axis near Canmore also contributing during the storm (fig. 5). Figure 6 illustrates that the June 2001 storm scored 0.5 for having an easterly component to the near-surface wind, and the June 2012 storm scored 2 points for having precipitable water content $\geq$ 20 kg m^{-2}, with its origins being both the subtropical Pacific and the Gulf of Mexico (fig. 7). The maximum score possible for one storm is 10.

Following this analysis, the storms could be classified somewhat, setting them apart according to their main mechanisms and contributing factors: upper-level low, upper-level low + subtropical or monsoonal moisture $\geq$ 20 kg m^{-2}, upper-level low + subtropical moisture $\geq$ 20 kg m^{-2} from Pacific **and** Gulf of Mexico, frontal, and main mechanism unclear.

The scoring system was an attempt to quantitively find a correlation between spatial features and the heavy rainstorm frequency or precipitation amount, but there is none obvious (fig. 8). Namely, several different types of synoptic weather systems can cause heavy precipitation near Canmore. Despite the attempt to include thunderstorms by using the lifted index, this is not well-modelled nor well-resolved by the coarse resolution reanalysis data (see appendix B), thereby contributing to this lack of correlation.

15 of 18 cases have upper-level closed lows, spanning all months in which the storms occurred, with 11 of them being quasi-stationary, and 1 of those associated with the passage of a frontal system. The deeper upper-level lows (low centre $\leq$ 5,500 m) all occurred between April and June, and the deeper surface lows (low centre $\leq$ 99.8 kPa) all occurred in May and June. Progressive frontal systems accounted for 3 cases, and despite tending to score lower, associated precipitation amounts were comparable to storms having different mechanisms, so they should not be discounted.

The storms that entrained large amounts of subtropical moisture occurred mostly since 1990, these being the highest scoring cases. This shows a potential shift in the large-scale pattern, bringing more moisture from the south (subtropics). However, the pattern is not completely new, because the 1952 case included subtropical moisture. Also, there are four storms, including the June 2013 storm, in which moisture was advected from both the subtropical Pacific Ocean and the Gulf of Mexico. This did not occur before 1990 (for these cases).

Judging by the spatial analysis of large-scale features, the June 2013 event was not unique, with similar storms occurring in 1990, 1995, 1998, 2005, and 2012. As discussed, one explanation for the greater precipitation amounts in 2013 is thunderstorms. These are not well accounted for in this analysis. Also, the scoring system is rather subjective and definitely does not account for all the variance.

Temporal analysis on the precipitation data is carried out in the next section.

b. Temporal analysis

The return period, RP, of a heavy precipitation event can be calculated using the following equation:

$$RP = \frac{N}{\sum_{i=1}^{N} f_i} \tag{1}$$

where f_i is the event frequency for N years ($i = 1,N$). Using all precipitation data in the period 1952–2013, we computed RP for 1981–2013, with a sliding window of $N = 30$ years (the standard time period to define a climatological average) using a 1-year interval (fig. 9). From 1982–1989, $RP = 6$ years, meaning that the probability of a heavy precipitation event occurring in one of those years is 1/6. From 2007–2013, $RP \leq 3$ years, and there is a clear downward trend in between these two time periods. This implies that heavy precipitation events are now approximately twice as likely to occur as they were 30 years ago.

c. Investigation into the correlation of heavy precipitation events with natural climate cycles

1) El Niño Southern Oscillation

El Niño Southern Oscillation (ENSO) events have historically been related to regional extremes in weather, such as hurricanes, droughts, and floods (Hanley et al. 2003). ENSO events tend to last 6–18 months, their fingerprint is seen mainly in the tropics, and the mechanisms are relatively well understood (Mantua and Hare 2002).

Several indices are commonly used to classify ENSO events, including averaged sea-surface temperature (SST) anomalies over at least six different regions in the tropical Pacific, to the surface atmospheric pressure-based index, as well as the multivariate ENSO index (MEI), which includes sea-level pressure, zonal and meridional surface wind components, SST, surface air temperature, and total cloud fraction. Based upon analysis of these indices, ENSO can be classified into three phases: warm (El Niño), cold (La Niña) and neutral.

To determine a warm (cold) phase, Trenberth (1997) recommends using data from the region bounded by 5°N–5°S, 120°–170°W known as Niño 3.4, with the Japanese Meteorological Agency (JMA) definition that 5-month running means of monthly SST anomalies must be greater than (less than) a certain threshold for at least six consecutive months. The MEI approach claims to provide a more complete and flexible description of ENSO than with using just one variable (Wolter and Timlin 2011). The correlation coefficient between the Niño 3.4 and the MEI indices is $r = 0.88$, giving confidence in their use yet showing enough difference to assess both.

The Niño 3.4 SST anomalies and MEI indices (5-month running means) are calculated for the entire period (1952–2013) (fig. 10). Threshold values used to classify the ENSO phase are determined using the upper quartile to define an El Niño event, and the lower quartile to define a La Niña event (Hanley et al. 2003). [The upper (lower) quartile for the Niño 3.4 SST anomalies is 0.57°C (−0.56°C), and the upper (lower) quartile for the MEI indices is 0.62 (−0.59) (dimensionless).]

The heavy precipitation events are also plotted in figure 10. With the Niño 3.4 data, 12 precipitation events occurred during a neutral ENSO phase, 4 at the end of an El Niño, in April, May or June, and 2 during the onset of a La Niña, in August and September. With the MEI data, 15 precipitation events occurred during a neutral phase, 2 at the end of an El Niño in May and June, and 1 in the 14th month (August) of a cold phase which persisted for 34 months.

Based upon this analysis, there is no direct correlation between ENSO phase and southern AB heavy precipitation events as defined in this study. When a heavy precipitation event did coincide with El Niño conditions, it was at the end of the warm phase during springtime. Similarly, when a precipitation event coincided with La Niña conditions, it was during the onset of the cold phase in August or September. However, all precipitation events occurred between April and September, with 14 of 18 events in May or June, so the ENSO data does not necessarily add to their predictability, since they are expected at this time of year anyway.

2) Pacific Decadal Oscillation

The Pacific Decadal Oscillation (PDO) can be observed by regime shifts in ENSO indices. Events persist for 20–30 years, the effects are mainly seen in the extratropics, particularly the North Pacific [it is strongly correlated with the Aleutian Low (Mantua et al. 1997)], and finally the mechanisms causing PDO variability are not well known (Mantua and Hare 2002). Regimes are commonly reported in the literature as follows: warm phase from 1925–1946 (prior to the dates used in this study, 1952–2013), cold phase from 1947–1976 (Bonsal and Shabbar 2011; Gan et al. 2007; Mantua and Hare 2002; Zhang et al. 1997), warm phase from 1977 onwards, with possible flip to cold phase in 1998 (Gan et al. 2007). It remains to be seen whether 1998 marks the beginning of 20–30 year cold phase (Mantua and Hare 2002).

The PDO Index uses North Pacific Ocean (poleward of 20°N) SST anomalies from 1900–1993 (Mantua 2000). Monthly mean global average SST anomalies are removed. The correlation coefficient between the 5-month running mean PDO and MEI (Niño 3.4) indices is $r = 0.63$ ($r = 0.51$) so we chose to compare the PDO and MEI indices (fig. 11). The regime shift to warm PDO phase in 1977 can be observed, as well as a sharp change in 1998.

Several periods within the phases determined in the literature could be considered significant shifts, e.g. in 1957–1958. The subsequent warm period lasted only a few years which is perhaps why it has received little emphasis in previous studies (Zhang et al. 1997). Strongly negative values at the end of the 1980s and early 1990s are also generally ignored in the modal classification of the PDO.

There appears to be no correlation between the literature-defined PDO epochs above and heavy precipitation events. Six events occur during the initial cold (negative) phase. Despite a break in precipitation events that seems to correspond with the proposed 1977 regime shift, 4 events occur between 1990 and 1998, while the PDO index is still positive. The remaining 8 events happen during what the literature considers a PDO cold phase. Judging by the

PDO index alone, 9 events occur during a warm phase, and 9 during a cold phase.

The apparently random spread of heavy precipitation events throughout all ENSO/PDO modes (since 1952) agrees with the findings of Gan et al. (2007) and Bonsal and Shabbar (2011), that relationships between ENSO/PDO and Canadian climate are strongest during the winter, and that the more consistent impacts are on temperature variables, and to a lesser extent precipitation. In particular, Gan et al. (2007) found that no single climate index can explain more than 30% of interannual precipitation variability in southwest Canada.

Their study region extended from BC across to Manitoba and they included complete precipitation records (not just heavy rain events) from 21 weather stations. With this in mind, accurate seasonal predictions of highly nonlinear precipitation processes are unlikely, using climate indices alone. This is supported by Yarnal and Diaz (1986), who claim that teleconnection patterns mainly capture the large-scale features of variability while local changes in anomaly centres can result in large differences in western North American climate.

Several studies claim that there is an enhancing effect on precipitation response in Canada when ENSO and PDO warm or cold phases coincide (Bonsal and Shabbar 2011; Gan et al. 2007; Mantua et al. 1997). This is not evident for the 18 heavy precipitation events in this study, since only 3 of them were during a potential "enhanced" ENSO and PDO phase, 1 cold and 2 warm (August 1974, and May and June 1998, respectively). There are several other occasions when potential enhancing occurs (fig. 11) but heavy precipitation events do not, such as 1957, 1977, 1983, 1987, to name a few.

Aside from occurring predominantly in winter, correlations between ENSO/PDO and precipitation appear to be with more stratiform than convective storms (Yarnal and Diaz 1986). Since thunderstorms are not well accounted for in this study, and precipitation amounts (fig. 3) do not correlate well with the large-scale analysis scoring system (fig. 8), this speculation could help explain why very little correlation is seen between ENSO/PDO and the 18 heavy precipitation events.

4. Summary and Conclusions

a. Summary

Precipitation data from three southern AB stations were used to identify 18 heavy precipitation events, with total precipitation $\geq$ 50 mm/(2 days), from 1952–2013. All cases occurred between April and September, with most storms in May and June. Precipitation amounts per storm were between 50–100 mm, except for three cases, two in 2005 and one in 2013 (this was the June 2013 event, precipitation at Kananaskis exceeded 270 mm).

Reanalysis maps of geopotential height, mean sea-level pressure, wind speed and direction, best 4-layer lifted index, precipitable water, and corrected precipitation rate, were used to intercompare these storms and score them based upon features known to bring heavy precipitation to southern AB. As a result of this classification scoring, most heavy precipitation events occurred due to a slow-moving upper-level closed low.

Also, the deepest low-pressure systems (considering upper and lower levels) occurred between April and May. Since 1990, there is a more regular occurrence of storms tapping moisture from the subtropics, and in particular, new occurrences (for this data) of storms sourcing moisture from both the subtropical Pacific Ocean and the Gulf of Mexico (the highest scoring storms, which includes the June 2013 event). 50% of cases since 1990 included subtropical moisture, as opposed to 39% for the entire 62-year period.

More progressive frontal systems as the main mechanism were rare (3 cases), but brought as much, sometimes more, precipitation as slower-moving storms, so should not be ignored. Some of the disparity between the scoring and precipitation amounts can likely be accounted for by thunderstorms that were not modelled or resolved by the coarse-resolution reanalysis data (this could also be the reason that no storms scored a maximum of 10 points, e.g. the June 2012 storm scored 9 but lacked instability according to the reanalysis data).

The return period of the heavy precipitation events was calculated with a 30-year sliding window and a 1-year interval. A downward trend is observed, from about 6 years in the

1980s to about 3 years from 2007–2013.

Two El Niño Southern Oscillation indices (El Niño 3.4 and MEI) were calculated to determine ENSO phases for the period 1952–2013, but no obvious correlation with heavy precipitation events was found. For the precipitation events that coincided with an ENSO phase (only 6 cases for El Niño 3.4 data), they were either at the end of a warm phase or the onset of a cold phase. However, these times are during spring or autumn when we can expect heavy precipitation events to occur anyway.

There is also no obvious correlation between the Pacific Decadal Oscillation and heavy precipitation events. Some correlation between PDO and precipitation in southwest Canada is reported in the literature for winter and for more stratiform than convective storms.

b. Conclusions and further work

- Most heavy precipitation events that have occurred in southern AB are caused by an upper-level quasi-stationary closed low, as opposed to any other mechanism. The next most important factors are subtropical moisture source(s), and easterly upslope flow/instability. All of these contributed to the June 2013 event.

- There is evidence of a change in the large-scale pattern, with more storms tapping moisture from the subtropics since 1990, in particular from both the Pacific Ocean and the Gulf of Mexico.

- Heavy precipitation events, as defined in this study, are about twice as likely to occur now (having a return period of about 3 years) as 30 years ago.

- A correlation cannot be found between heavy precipitation events and large scale climate signals, specifically the ENSO and the PDO. When they did coincide with ENSO, the timing was consistent, so this is worth investigating further.

- It is not appropriate to use climate indices alone to capture the variability in the spring/summer heavy precipitation events in this study, many of which have a strong convective component.

This study is somewhat limited by defining heavy precipitation events, thereby reducing available precipitation data substantially. With regards to correlation with climate signals, we suggest that future work includes more precipitation data (more stations and possibly no thresholds) to investigate this thoroughly, and this is beyond the scope of the analysis here.

In addition, further work could include analysis of a higher-resolution dataset in an attempt to better include thunderstorms (instability). The higher resolution data currently available (North American Regional Reanalysis) only dates back to 1977, so it was not included in this study, as this would have reduced the (already small) number of heavy precipitation cases.

We also recommend that a high-quality automatic weather station be installed at Canmore. It would aid in documenting high-precipitation/flood events and could have other advantages for the Town regarding road maintenance, health, and other issues.

Acknowledgments.

For the use of NCEP/NCAR reanalysis data, we thank Dr. Christopher Godfrey, the University of North Carolina Asheville, and the National Centers for Environmental Prediction/National Center for Atmospheric Research. NCEP Reanalysis data was provided by the NOAA/OAR/ESRL PSD, Boulder, Colorado, USA, from their website at http://www.esrl.noaa.gov/psd/.

Regarding the use of EC Climate Data Online: the website is official work that is published by the Government of Canada, and the reproduction has not been produced in affiliation with or with the endorsement of the Government of Canada.

Thanks to Matthias Jakob of BGC Engineering Inc. for spearheading this project, and to Andy Esarte at Canmore, AB, for organizing the funding for this work.

APPENDIX A

Adjusted and Homogenized Canadian Climate Data

The Adjusted and Homogenized Canadian Climate Dataset (AHCCD) was created for use in climate research. Adjustments are applied to original station data to account for shifts due to instrument changes and observing procedures. Mekis and Vincent (2011) describe the corrections to precipitation records, in particular due to wind undercatch, evaporation, and gauge-specific problems.

Of the three stations in this study, only Banff is included in the AHCCD, and only monthly rain records are available up to 2007. For the 12 months within the AHCCD that contain heavy precipitation events (some months had more than one event), the mean absolute difference between original rain record and adjusted totals is 7.3 mm, with a standard deviation of 2.2 mm. Since this discrepancy is small and we do not know when within the month the correction is applied, we chose to use the original Banff record, which contributed to identifying 8 of the 18 heavy precipitation events.

APPENDIX B

Definitions and details of reanalysis variables

a. Geopotential heights (m) at at altitude of roughly 5.5 km, where pressure is 50 kPa. Designated a class A variable by NCEP/NCAR, which is the most reliable class, strongly influenced by observational data.

b. Mean sea level pressure (hPa) (class A).

c. Wind speed (m s^{-1}) and direction interpolated to a near-surface reference pressure of 100 kPa (class A).

d. Best 4-layer lifted index (°C) (Galway 1956; DeRubertis 2006). Designated a Class B variable, meaning there are observational data directly affecting the value but the numerical weather prediction (NWP) model has a very strong influence on the analysis value. The lifted index, an indication of atmospheric stability, is based upon the difference between the temperature at 50 kPa and the temperature of a parcel of air lifted to 50 kPa. The more negative the temperature difference is, the greater the chance of thunderstorms (the warmer the parcel is than the environment). For the best 4-layer lifted index, the lifted index is found by lifting from 4 different levels between the surface and 1600 m altitude, and the "best" or most unstable value is kept. This can eliminate times when the surface value may misrepresent the true (deep-layer) instability. Factors leading to a low lifted index value are cold air aloft, large low-level moisture, and a warm surface temperature, for which the latter two variables may not be well modelled in the reanalysis.

e. Precipitable water (kg m^{-2}). This is the amount of water vapour in an atmospheric column, integrated between the surface and 10 hPa (∼40 km) (Class B).

f. Corrected precipitation rate (cm day^{-1}). Designated a Class C variable, which is not directly affected by observations but derived solely from model fields forced by data assimilation to remain in balance with the atmosphere. Due to this class being more unreliable and smoothing by the NWP model, precipitation data was only used to build confidence in the EC data as to the timing of the heavy precipitation events. Accuracy in rainfall intensity for the NCEP/NCAR data was neglected.

APPENDIX C

Other definitions

- Z = Zulu time = coordinated universal time (UTC). UTC = MST + 7 hours.
- mb = millibars, an outdated pressure unit used on some old weather maps.

  1000 mb = 1000 hPa = 100 kPa.

REFERENCES

Bonsal, B. and A. Shabbar, 2011: Large-scale climate oscillations influencing Canada, 1990–2008. Tech. rep., Canadian Councils of Resource Ministers.

DeRubertis, D., 2006: Recent Trends in Four Common Stability Indices Derived from U.S. Radiosonde Observations. *J. Climate*, **19 (3)**, 309–323, URL http://dx.doi.org/10.1175/JCLI3626.1, doi: 10.1175/JCLI3626.1; M3: doi: 10.1175/JCLI3626.1; 31.

EnvironmentCanada, 2013: National Climate Data and Information Archive Website. URL http://www.climate.weatheroffice.gc.ca/climateData/canada_e.html, URL http://www.climate.weatheroffice.gc.ca/climateData/canada_e.html.

Galway, J. G., 1956: The lifted index as a predictor of latent instability. *Bull. Am. Meteorol. Soc.*, **37**, 528–529.

Gan, T. Y., A. K. Gobena, and Q. Wang, 2007: Precipitation of southwestern Canada: Wavelet, scaling, multifractal analysis, and teleconnection to climate anomalies. *J. Geophys. Res. Atmos.*, **112 (D10)**, n/a–n/a, URL http://dx.doi.org/10.1029/2006JD007157.

Godfrey, C., 2010: NCEP Reanalysis Plotter. URL http://www.atms.unca.edu/cgodfrey/reanalysis/reanalysis.shtml, URL http://www.atms.unca.edu/cgodfrey/reanalysis/reanalysis.shtml.

Hanley, D. E., M. A. Bourassa, J. J. O'Brien, S. R. Smith, and E. R. Spade, 2003: A Quantitative Evaluation of ENSO Indices. *J. Climate*, **16 (8)**, 1249, URL http://search.ebscohost.com/login.aspx?direct=true&db=a2h&AN=9465131&site=ehost-live&scope=site, m3: Article.

Kalnay, E., et al., 1996: The NCEP/NCAR 40-Year Reanalysis Project. *Bull. Am. Meteorol. Soc.*, **77 (3)**, 437–471, URL `http://dx.doi.org/10.1175/1520-0477(1996)077<0437:TNYRP>2.0.CO;2`, doi: 10.1175/1520-0477(1996)0772.0.CO;2; M3: doi: 10.1175/1520-0477(1996)0772.0.CO;2; 13.

Mantua, N., 2000: The Pacific Decadal Oscillation. URL `http://jisao.washington.edu/pdo/`, URL `http://jisao.washington.edu/pdo/`.

Mantua, N. and S. Hare, 2002: The pacific decadal oscillation. *Journal of Oceanography*, **58 (1)**, 35–44, URL `http://dx.doi.org/10.1023/A%3A1015820616384`, j2: Journal of Oceanography.

Mantua, N. J., S. R. Hare, Y. Zhang, J. M. Wallace, and R. C. Francis, 1997: A Pacific Interdecadal Climate Oscillation with Impacts on Salmon Production. *Bull. Am. Meteorol. Soc.*, **78 (6)**, 1069–1079, URL `http://dx.doi.org/10.1175/1520-0477(1997)078<1069:APICOW>2.0.CO;2`, doi: 10.1175/1520-0477(1997)0782.0.CO;2; M3: doi: 10.1175/1520-0477(1997)0782.0.CO;2; 27.

Mekis, E. and L. Vincent, 2011: An Overview of the Second Generation Adjusted Daily Precipitation Dataset for Trend Analysis in Canada. *Atmos. Ocean*, **2**, 163–177.

NCEP/NCAR, 2014: NCEP/NCAR Reanalysis 1 Data. URL `http://www.esrl.noaa.gov/psd/data/gridded/data.ncep.reanalysis.html`, URL `http://www.esrl.noaa.gov/psd/data/gridded/data.ncep.reanalysis.html`.

Trenberth, K. E., 1997: The Definition of El Niño. *Bull. Am. Meteorol. Soc.*, **78 (12)**, 2771–2777, URL `http://dx.doi.org/10.1175/1520-0477(1997)078<2771:TDOENO>2.0.CO;2`, doi: 10.1175/1520-0477(1997)0782.0.CO;2; M3: doi: 10.1175/1520-0477(1997)0782.0.CO;2; 25.

Wolter, K. and M. S. Timlin, 2011: El Niño/Southern Oscillation behaviour since 1871 as diagnosed in an extended multivariate ENSO index (MEI.ext). *Int. J. Climatol.*, **31 (7)**, 1074–1087, URL http://dx.doi.org/10.1002/joc.2336.

Yarnal, B. and H. F. Diaz, 1986: Relationships between extremes of the Southern oscillation and the winter climate of the Anglo-American Pacific Coast. *J. Climatol.*, **6 (2)**, 197–219, URL http://dx.doi.org/10.1002/joc.3370060208.

Zhang, Y., J. Wallace, and D. Battisti, 1997: ENSO-like Interdecadal Variability: 1900–93. *J. Climate*, **10**, 1004–1020, URL http://dx.doi.org/10.1175/1520-0442(1997)010%3C1004:ELIV%3E2.0.CO;2, iD: 3255.

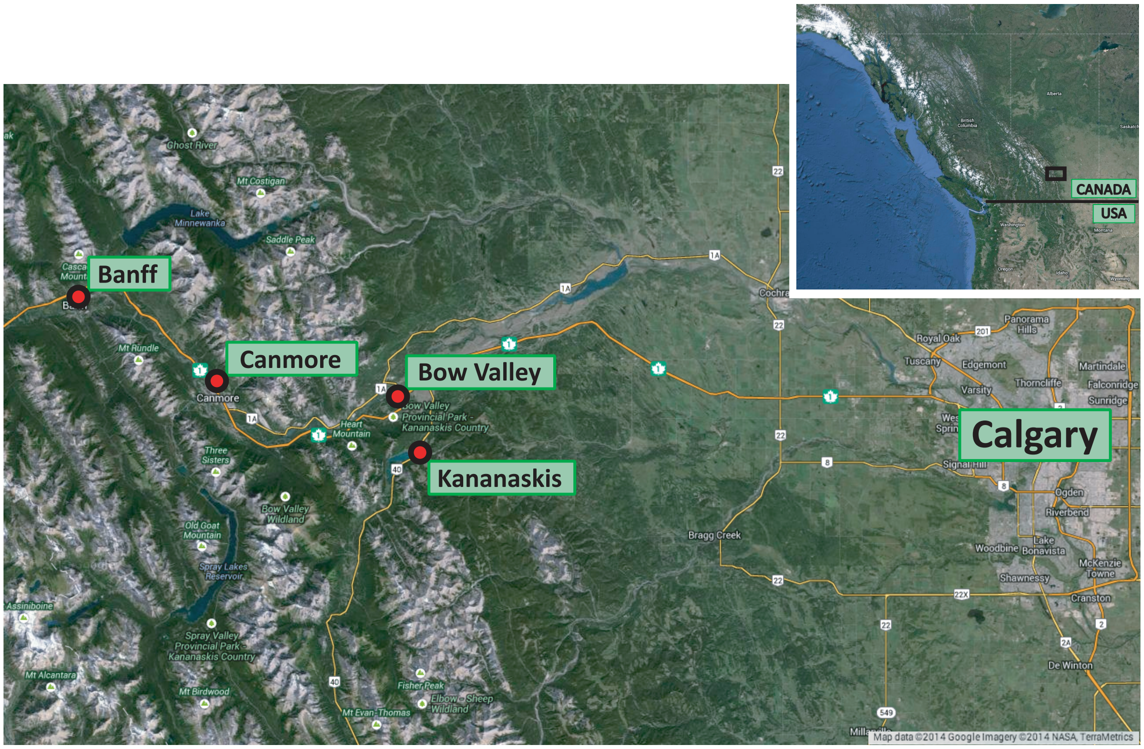

Fig. 1. Map showing locations affected by the June 2013 storm and local Environment Canada weather station locations (Banff, Bow Valley, and Kananaskis) providing monthly and daily precipitation data. (Map data from 2014 Google Imagery.)

Table 1. Automatic weather stations near Canmore providing historical monthly and daily precipitation data. Banff and Bow Valley stations were moved during the record, but within close enough proximity to the old station to be considered a continuous record for the purposes of this report.

Station name	Latitude (N)	Longitude (W)	Elevation (ASL)	Record
Banff	51°11’00”	115°34’00”	1383.7 m	1887–1995
Banff CS	51°11’36”	115°33’08”	1396.9 m	1995–present
Bow Valley Prov. Park	51°05’00”	115°04’00”	1318.0 m	1967–1990
Bow Valley	51°05’00”	115°04’00”	1297.5 m	1993–present
Kananaskis	51°01’39”	115°02’05”	1391.1 m	1939–present

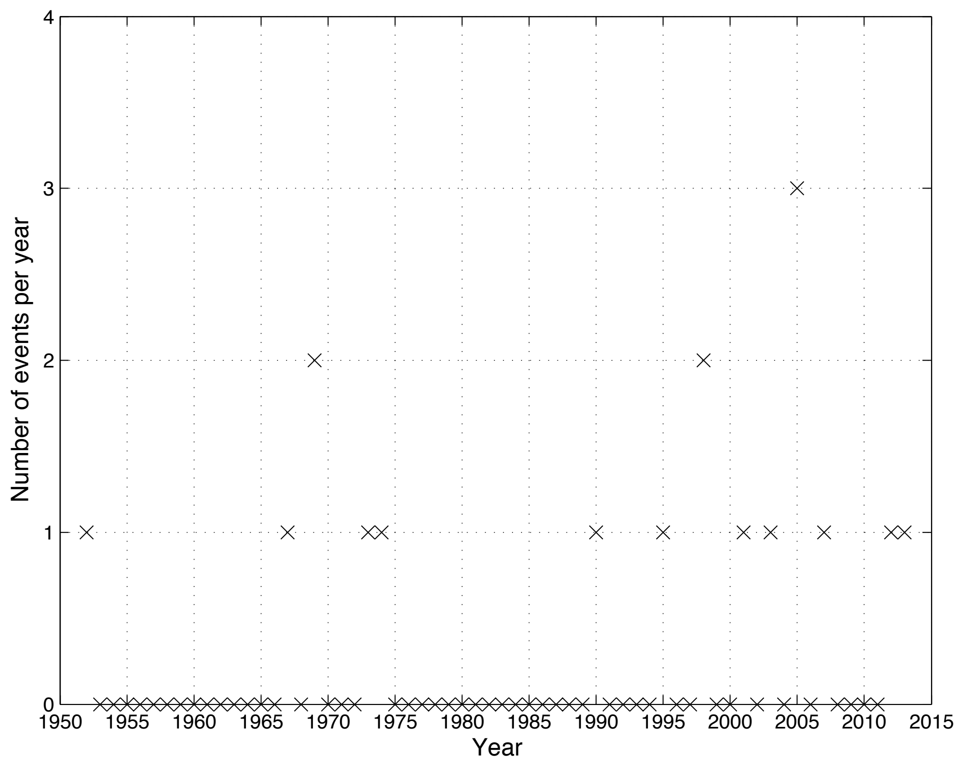

FIG. 2. Frequency of heavy precipitation events per year for the Canmore area, using historical data from Banff, Bow Valley, and Kananaskis stations, between 1952–2013. A heavy precipitation event is defined by total rainfall $\geq$ 50 mm/(2 days) for at least two of the three stations.

TABLE 2. Dates and details of each heavy precipitation event. Storms that had total rainfall $\geq$ 50 mm/(2 days) at all three stations are in bold. Values in parentheses are precipitation totals during the storm that do not reach an excess of 50 mm in the required 2 days for this study. Also noted are some examples of important mechanisms and factors contributing to each storm. For the data in this table, surface lows were centred near to Canmore, easterly flow was present at upper and lower levels, and large amounts of moisture came from the subtropics (Pacific Ocean and Gulf of Mexico). UL = upper-level.

Year	Dates	Rain total per storm (mm)			Main mechanisms and contributing factors					
		Banff	Bow Valley	Kananaskis	UL low	UL trough	Surface low	Easterly flow	Moisture	Front
1952	June 21–23	54.8	-	86.1	×		×		×	
1967	May 29–30	(29.2)	55.1	65.6	×	×		×		
1969	June 23–24	(17.0)	62.4	67.6		×				×
1969	June 27–28	(23.1)	62.5	59.2	×	×				
1973	May 24–26	50.1	(52.3)	68.6		×				×
1974	August 11–13	(35.3)	57.6	63.5		×				
1990	May 24–25	51.4	73.0	(44.0)	×	×	×	×	×	
1995	September 4–6	(26.8)	63.4	94.2	×	×			×	
1998	May 26–28	(31.0)	51.0	73.4	×	×			×	
1998	June 17–19	(13.1)	64.0	94.6	×					×
2001	June 2–7	(6.6)	57.8	73.2	×	×		×		
2003	**April 24–25**	**57.8**	**58.4**	**60.4**	×					
2005	June 5–8	(52.6)	120.3	137.0	×					
2005	**June 16–18**	**106.8**	**119.4**	**149.2**	×				×	
2005	September 8–10	51.2	(63.8)	102.8	×	×				
2007	June 15–17	(30.6)	78.2	90.0	×					
2012	**June 4–6**	**69.5**	**64.7**	**86.2**	×	×	×	×	×	
2013	**June 18–21**	**90.9**	**219.3**	**272.4**	×		×	×	×	

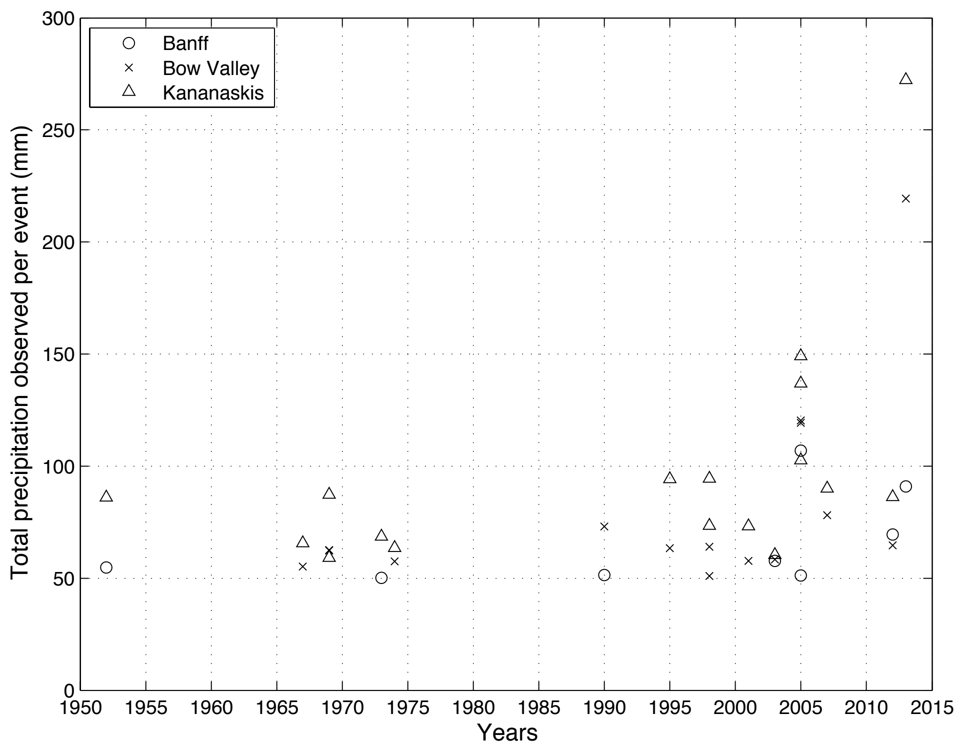

FIG. 3. Precipitation totals at each station, Banff, Bow Valley, and Kananaskis, for the 18 heavy precipitation cases. Note that some years have more than one heavy precipitation event.

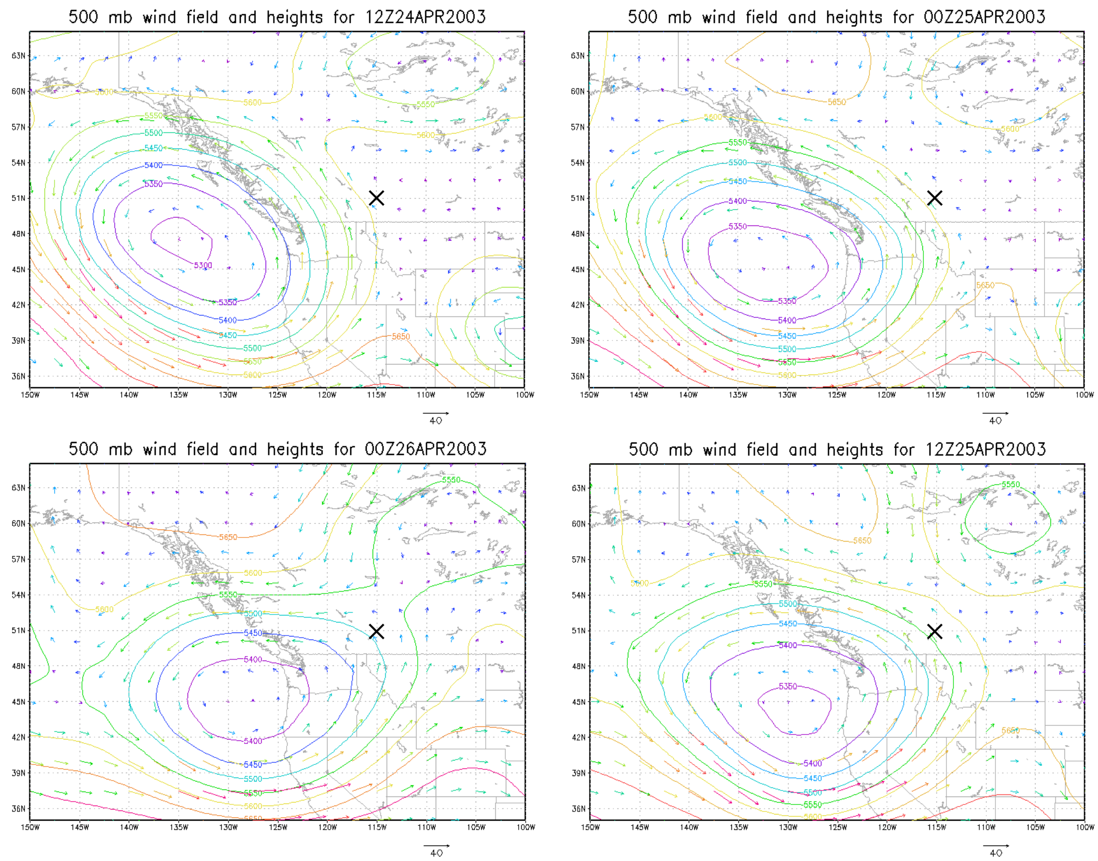

Fig. 4. 50 kPa geopotential heights (contours in metres) and wind direction (vectors) for the April 2003 storm, clockwise from top left: 12Z on 24 April 2003, 00Z on 25 April 2003, 12Z on 25 April 2003, and 00Z on 26 April 2003. A quasi-stationary upper-level low-pressure system is shown, scoring 2.5 points by the scoring system in the text. Canmore is situated at approximately 51°N, 115°W, as indicated with ×.

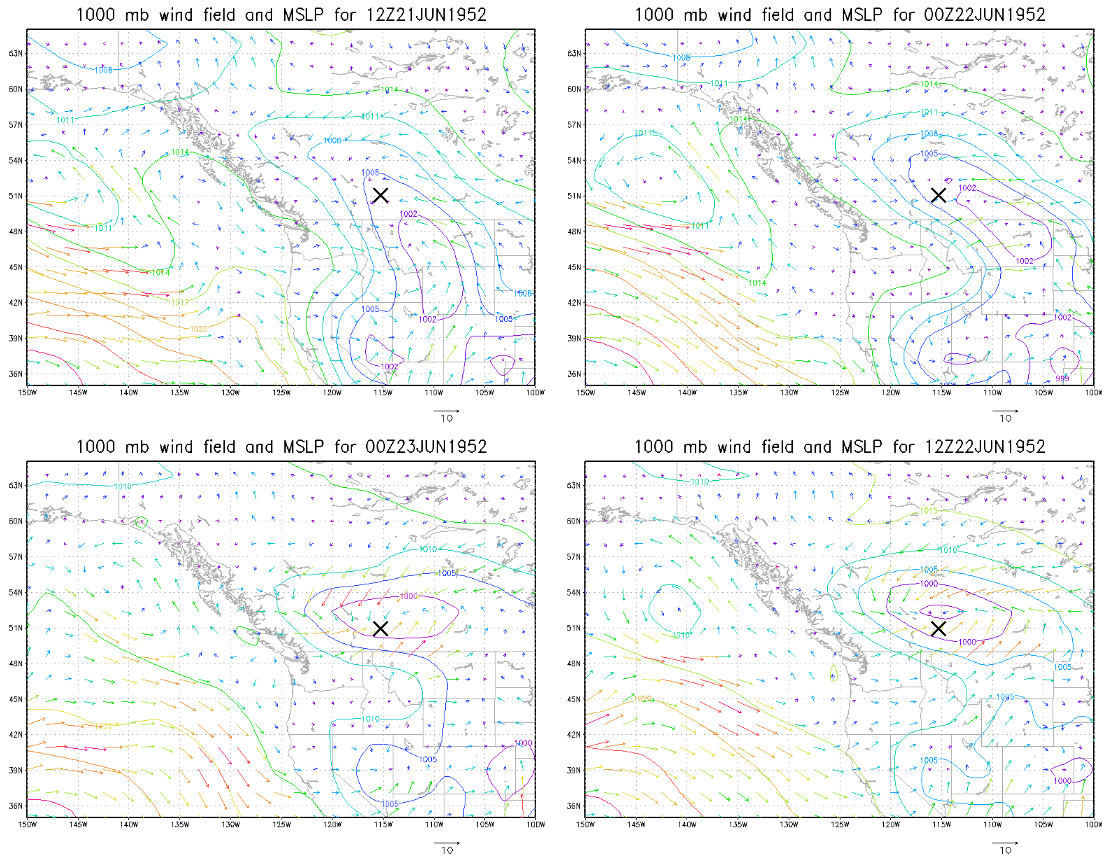

FIG. 5. Mean sea-level pressure (contours in hPa) and wind direction (vectors) for the June 1952 storm, clockwise from top left: 12Z on 21 June 1952, 00Z on 22 June 1952, 12Z on 22 June 1952, and 00Z on 23 June 1952. Surface troughing in the lee of the Canadian Rockies is shown, with a quasi-stationary surface low-pressure system, scoring 2.5 points. Canmore is situated at approximately 51°N, 115°W, marked with ×.

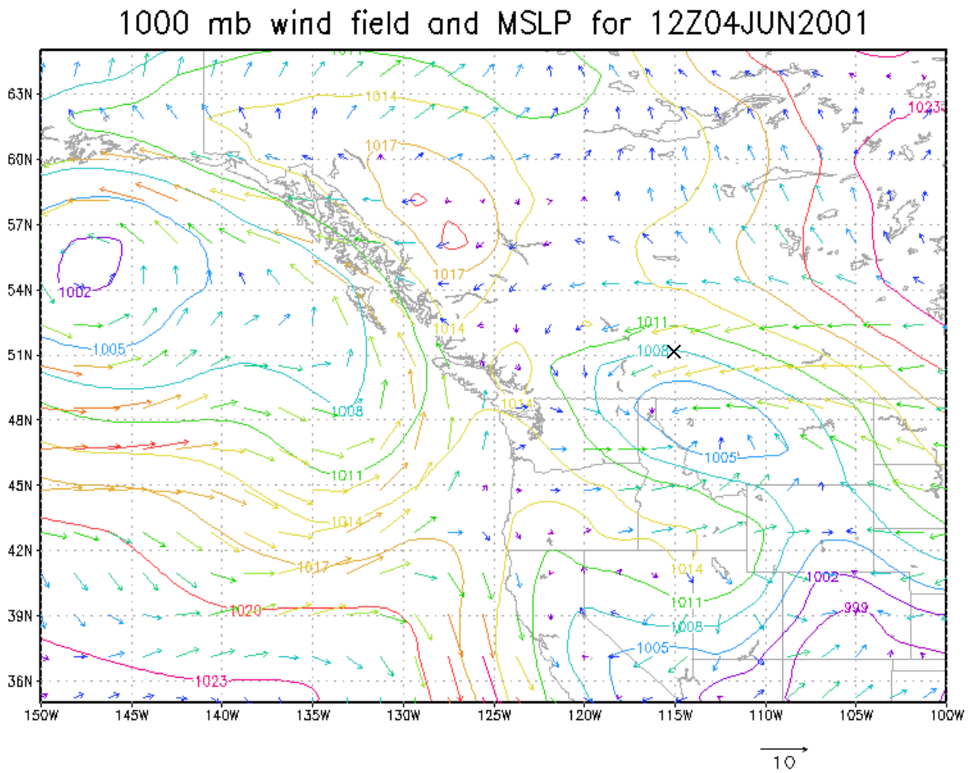

Fig. 6. Mean sea-level pressure (contours in hPa) and wind direction (vectors) for the June 2001 storm (shown here at 12Z on 4 June 2001). An easterly component to the surface winds is evident in the Canmore area and to the lee of the Canadian Rockies, scoring 0.5. Canmore is situated at approximately 51°N, 115°W, marked with ×.

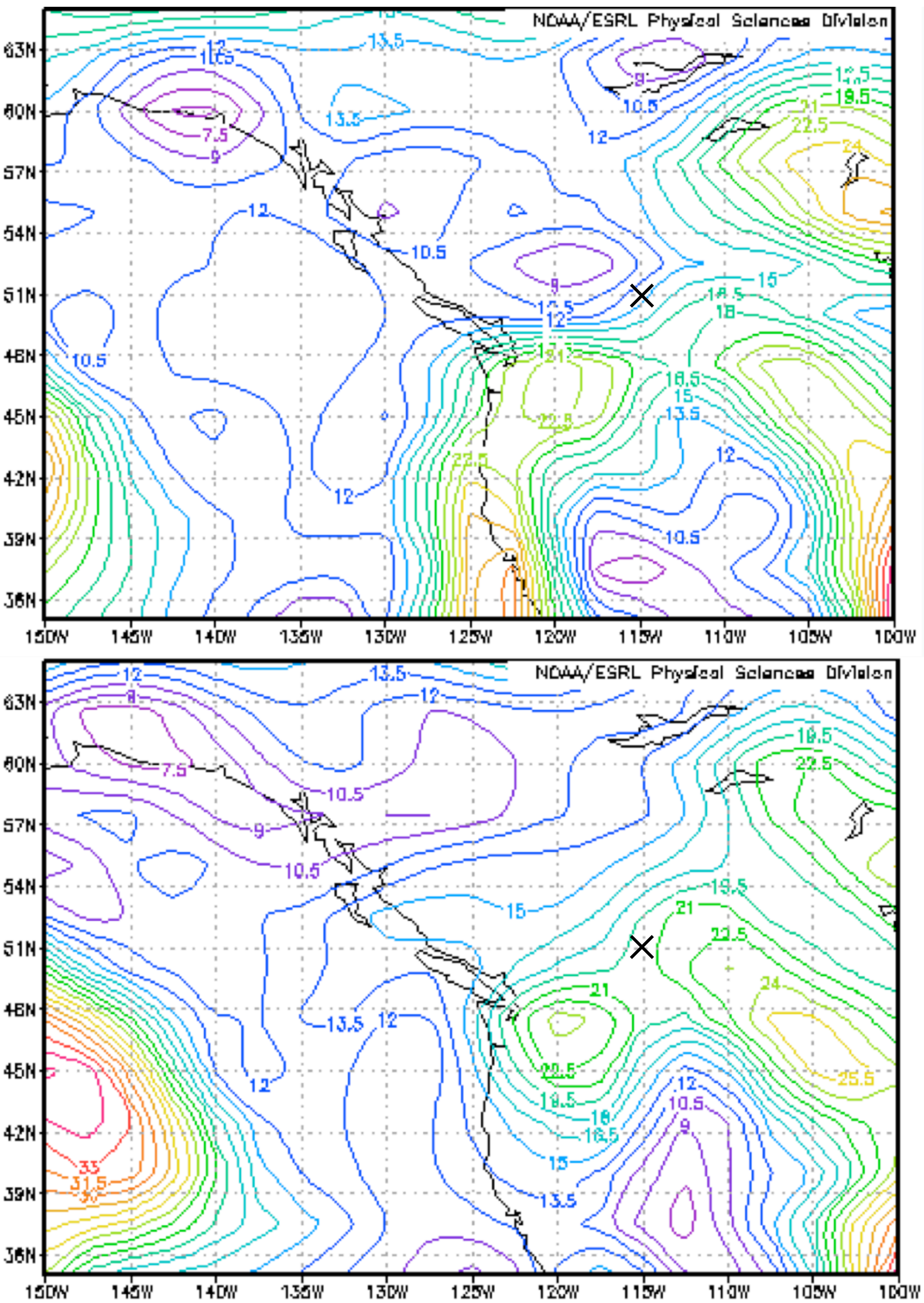

FIG. 7. Precipitable water content (contours in kg m^{-2}) for the June 2012 storm. Top: 12Z on 4 June 2012, bottom: 00Z on 5 June 2012 (12 hours later). Canmore is situated at approximately 51°N, 115°W (indicated by ×), with the moisture source advected towards it from the subtropical Pacific and the Gulf of Mexico.

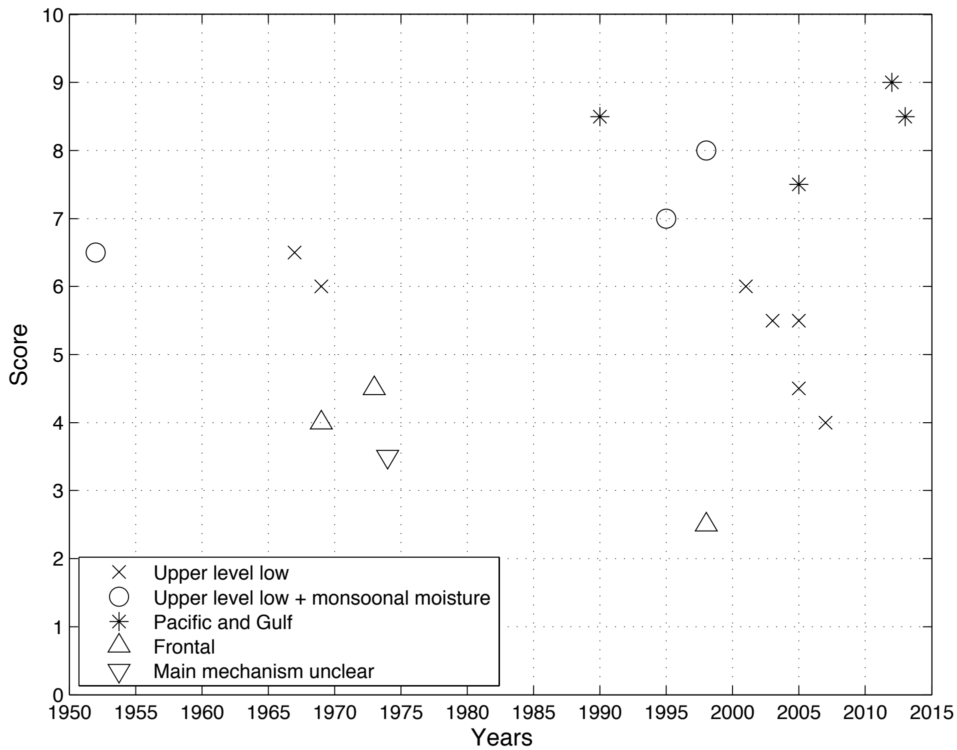

Fig. 8. Total score of each heavy precipitation event according to the rating in the text, plotted by category: upper-level low (crosses), upper-level low plus subtropical moisture greater than 20 kg m^{-2} (open circles), upper-level low plus subtropical moisture greater than 20 kg m^{-2} from Pacific **and** Gulf of Mexico (asterisks), frontal (upward triangles), and main mechanism unclear (downward triangle).

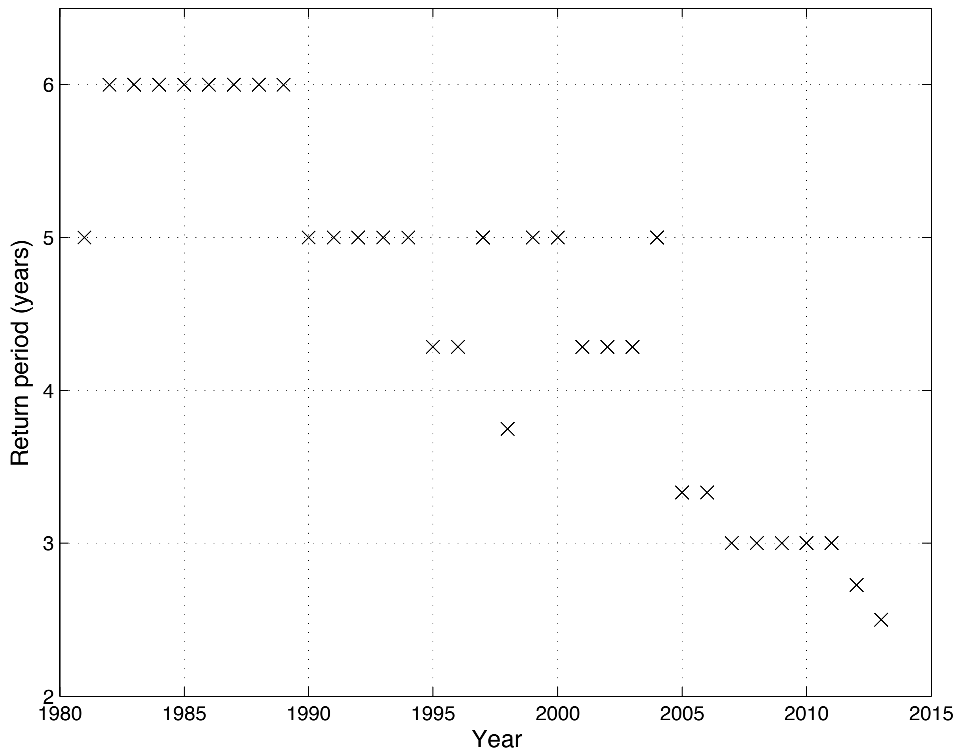

FIG. 9. Return period for heavy precipitation events (as defined in the text) using data from 1952–2013, 18 events in total. Sliding window size is 30 years with a 1 year interval. Each $\times$ corresponds to an average over the 30-year window, ending at the year marked by the $\times$.

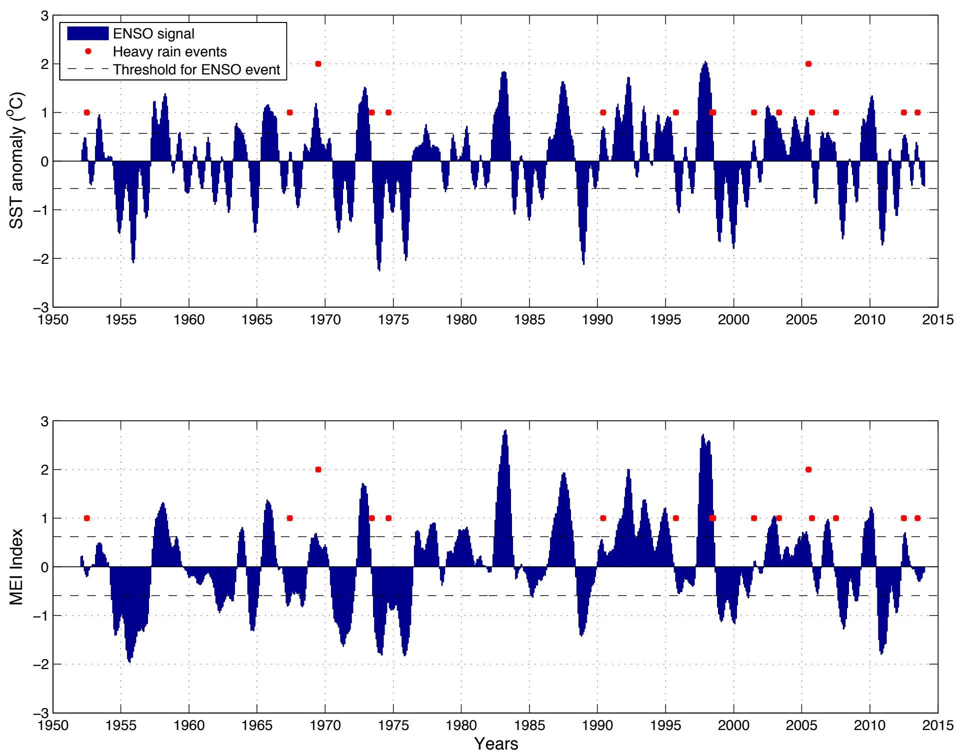

FIG. 10. Time series of the Niño 3.4 index (top panel) and the MEI index (bottom panel) in blue, with upper and lower quartiles (dashed lines) showing thresholds for determining a warm or cold ENSO phase, respectively. The count of southern AB heavy precipitation events is shown with red dots.

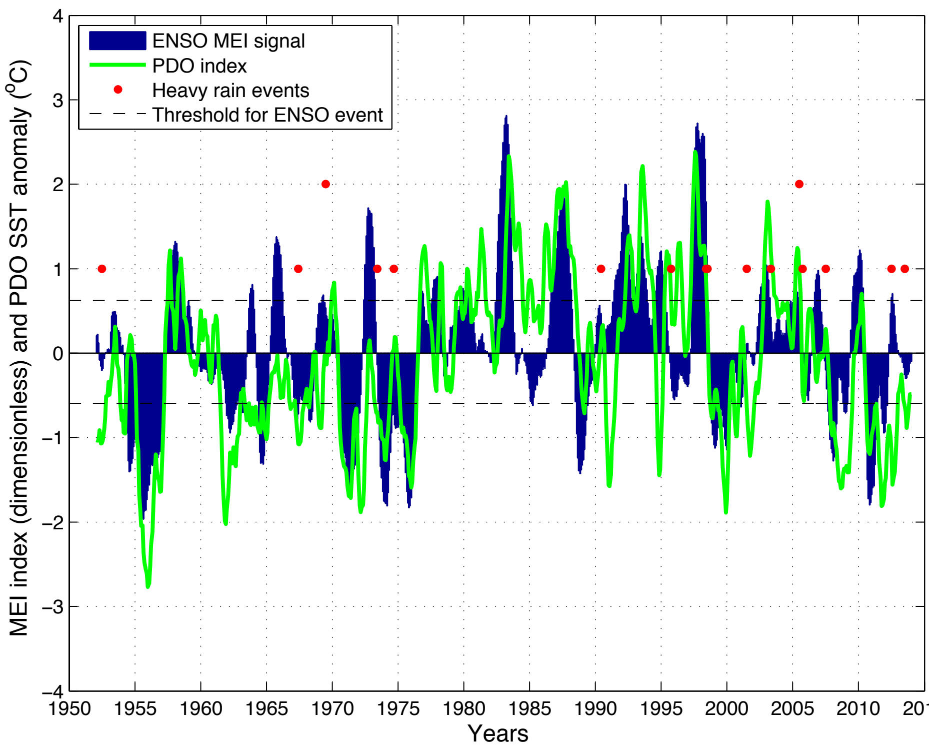

FIG. 11. Time series of the MEI (blue) and PDO (green) index, with upper and lower quartiles (dashed lines) showing thresholds for determining a warm or cold ENSO phase, respectively. The count of southern AB heavy precipitation events is shown with red dots.